Research in Astronomy and Astrophysics, 24:105001 (8pp), 2024 October https://doi.org/10.1088/1674-4527/ad7822

A Preliminary Comparative Study on the Centering Algorithms for Cassini-ISS NAC Images

T. Liang[1], Q.-F. Zhang[1,2], G.-M. Liu[3], W.-H. Zhu[1,2], and C.-S. Wang[1,2]
[1] Department of Computer Science, Jinan University, Guangzhou 510632, China; tqfz@jnu.edu.cn
[2] Sino-French Joint Laboratory for Astrometry, Dynamics and Space Science, Jinan University, Guangzhou 510632, China
[3] School of Computer Science, Guangdong University of Education, Guangzhou 510303, China
Received 2024 June 1; revised 2024 August 8; accepted 2024 September 4; published 2024 September 26

Abstract

Obtaining high precision is an important consideration for astrometric studies using images from the Narrow Angle Camera (NAC) of the Cassini Imaging Science Subsystem (ISS). Selecting the best centering algorithm is key to enhancing astrometric accuracy. In this study, we compared the accuracy of five centering algorithms: Gaussian fitting, the modified moments method, and three point-spread function (PSF) fitting methods (effective PSF (ePSF), PSFEx, and extended PSF (xPSF) from the Cassini Imaging Central Laboratory for Operations (CICLOPS)). We assessed these algorithms using 70 ISS NAC star field images taken with CL1 and CL2 filters across different stellar magnitudes. The ePSF method consistently demonstrated the highest accuracy, achieving precision below 0.03 pixels for stars of magnitude 8–9. Compared to the previously considered best, the modified moments method, the ePSF method improved overall accuracy by about 10% and 21% in the sample and line directions, respectively. Surprisingly, the xPSF model provided by CICLOPS had lower precision than the ePSF. Conversely, the ePSF exhibits an improvement in measurement precision of 23% and 17% in the sample and line directions, respectively, over the xPSF. This discrepancy might be attributed to the xPSF focusing on photometry rather than astrometry. These findings highlight the necessity of constructing PSF models specifically tailored for astrometric purposes in NAC images and provide guidance for enhancing astrometric measurements using these ISS NAC images.

Key words: methods: analytical – techniques: image processing – stars: imaging – astrometry

1. Introduction

The Cassini-Huygens mission, which launched on 1997 October 15, and ended on 2017 September 15, carried twelve instrument systems, including the Imaging Science Subsystem (ISS) which consisted of two optical cameras: the Wide-Angle Camera (WAC) and the higher-resolution Narrow-Angle Camera (NAC). The NAC, with a 2 m focal length and a $0\overset{\circ}{.}35$ field of view (Porco et al. 2004), captured the majority of images during the mission due to its superior resolution compared to the WAC. These images have been widely used in astrometric studies.

Notably, Cooper et al. (2006, 2014) reduced some ISS images of Jovian and Saturnian satellites, while Tajeddine et al. (2013, 2015) used ISS images to conduct astrometry of major Saturnian satellites. Zhang et al. (2018, 2021, 2022) performed astrometric analyses of ISS NAC images of Enceladus, Anthe, and Phoebe. Furthermore, Lainey et al. (2024) used Cassini ISS astrometry to establish that Mimas has a subsurface ocean. These studies have demonstrated the research value of high-precision astrometric positions derived from ISS NAC images.

Cooper et al. (2018) introduced Caviar, a dedicated astrometry package for ISS images that employs a Gaussian fitting method for centering. Zhang et al. (2021) conducted a comparative study between Gaussian fitting and the modified moments method, demonstrating that the latter provides better accuracy and precision. Both Gaussian fitting and the modified moments method are conventional algorithms for centering (Stone 1989), known for their simplicity and ease of implementation. Alternatively, point-spread function (PSF) methods, while more complex in application, are considered to offer higher accuracy and precision.

Anderson & King (2000) proposed a centering method based on the effective point spread functions (ePSF), significantly improving the centering accuracy for Hubble Space Telescope images. Zhang & Peng (2010) compared the ePSF and Gaussian fitting methods by simulating star images and found that both methods provide almost equal accuracy for well-sampled images. Bertin (2011) introduced the PSFEx software, presenting a novel centering technique in which the PSF is expressed by linear combinations of basis vectors, integrated into SExtractor, and widely adopted. Additionally, the Cassini Imaging Central Laboratory for Operations (CICLOPS) (West et al. 2010; Knowles et al. 2020) has released the extended PSFs (xPSF) for ISS NAC. These can also be employed for fitting to derive the centroid of point sources in ISS NAC images.

There are also specific centering methods, such as the fitting method based on Fourier space phase fitting introduced by Lu et al. (2018), and PSF-NET, a cycle convolutional neural network-based approach proposed by Jia et al. (2020). These algorithms often exhibit effectiveness in specific scenarios but lack the universal applicability of Gaussian, modified moments, and PSF fitting methods, which remain widely used and effective.

This study compares the performance of different centering methods in the astrometry of ISS NAC images. These methods include Gaussian fitting, modified moments, and three PSF fitting methods. We used star field images from the Cassini ISS NAC to perform the comparative experiment. Section 2 briefly introduces the five centering algorithms. Section 3 describes the comparative experiment. Section 4 details the results and analysis. Section 5 concludes the study.

2. Centering Algorithms

In this study, five centering algorithms were applied to ISS NAC images in order to conduct the comparison. Among these, Gaussian fitting is a commonly used and straightforward algorithm, which assumes that the PSF of a point source is a 2D Gaussian function. The modified moments method is also a simple and widely used algorithm. Zhang et al. (2021) pointed out that this method offers higher accuracy than Gaussian fitting for ISS NAC images. However, the modified moments method does not account for the shape of the PSF of the point source. In contrast, PSF fitting methods, which account for the actual shape of the PSF and use it to fit the star image to determine the centroid, are generally considered more accurate. There are various ways to obtain the PSF. The ePSF technique and PSFEx software are commonly used for acquiring the PSF, and thus we included both in our comparison. Additionally, extended PSFs (xPSFs) provided by CICLOPS for NAC images can be used to perform PSF fitting, so we included xPSF fitting in our analysis. These methods are detailed below.

2.1. Gaussian Fitting Method

The Gaussian fitting method primarily uses a two-dimensional Gaussian function to model the intensity distribution of a point source, with the coordinates of the function's peak serving as the centroid of the point source. Treating the CCD image's x and y coordinates as independent variables, and assuming rotational symmetry for the stellar intensity distribution, the intensity distribution $I(x, y)$ can be expressed as:

$$I(x, y) = B + H \times \exp\left\{-\frac{(x - x_c)^2 + (y - y_c)^2}{2R^2}\right\}. \quad (1)$$

In this model, B represents the sky background, and H is the peak value of the 2D Gaussian function, (x_c, y_c) are the coordinates of the centroid. R is the standard deviation of the Gaussian function.

2.2. Modified Moments Method

The modified moments method determines the center coordinates of an object by computing the first moment. The basic formula is as follows (Auer & van Altena 1978):

$$\begin{cases} x_0 = \dfrac{\sum\sum xG'(x, y)}{\sum\sum G'(x, y)} \\ y_0 = \dfrac{\sum\sum yG'(x, y)}{\sum\sum G'(x, y)}. \end{cases} \quad (2)$$

Here, $G'(x, y)$ is defined as:

$$G'(x, y) = \begin{cases} G(x, y) - T & G(x, y) > T \\ 0 & G(x, y) \leqslant T. \end{cases} \quad (3)$$

Here, $G(x, y)$ represents the grayscale value of the pixel at position (x,y), and T is the threshold. In our work, we have adopted the threshold setting proposed by Zhang & Peng (2010):

$$T = b + (\max - \min)k. \quad (4)$$

Here, b is the average sky gray value, max and min are the maximum and minimum grayscale values within the target frame containing the star image, and the coefficient k is determined by means of experimentation.

This method effectively filters out background noise by subtracting the threshold T from the grayscale values, focusing the calculation on the significant pixel values that represent the object of interest. By computing the weighted average of the pixel positions using these filtered values, the modified moments method provides accurate center coordinates for celestial objects.

2.3. Three PSF Fitting Methods

The PSF characterizes the diffraction and spreading of light during the transmission process. For an imaging system such as a CCD, when a point source of light serves as the input, the two-dimensional intensity distribution of that point source on the focal plane is the PSF. The PSF fitting technique models the images of celestial objects using the PSF to achieve a close approximation to the true observed image and accurately determine the centroid of celestial objects. This method involves constructing a PSF model and iteratively adjusting its parameters to match the actual image data closely.

Two prominent PSF fitting methods in astrometry are the ePSF technique introduced by Anderson & King (2000) and the PSFEx software developed by Bertin (2011). Both methods lead to excellent results in astrometric applications, achieving high precision for undersampled images. The ISS NAC images

in this study typically exhibit significant undersampling, with a full-width at half-maximum (FWHM) of only 1.3 pixels for images captured through the CL1 and CL2 filters. Theoretically, the ePSF and PSFEx methods are well-suited for astrometry of undersampled ISS NAC images.

In the ePSF method, let x_* and y_* denote a star centroid, p_{ij} is the gray value of the star image at (i, j), f_* represents the flux factor related to brightness (Here, we take it as peak gray value of the star.), $\psi_E(i - x_*, j - y_*)$ is the effective PSF, and s_* is the sky background. The gray distribution of a star is expressed as:

$$p_{ij} = f_* \psi_E(i - x_*, j - y_*) + s_*. \tag{5}$$

The PSF is constructed by iteratively fitting the gray values of many stars in the image, while simultaneously refining the centroid positions of individual stars. The sophisticated process has been implemented in the Photutils software package (Bradley et al. 2024). It allows us to leverage its robust ePSF generation capabilities while simultaneously extracting high-precision astrometric positions of stars in our ISS NAC images.

In the PSFEx method (Bertin 2011), the PSF model is expressed by a linear combination of basis vectors $\boldsymbol{\psi}_b$ which can be defined by users. That is, the PSF function ψ is expressed as: $\psi = \sum_b c_b \boldsymbol{\psi}_b$. The PSF and centroids of stars are achieved by minimizing the χ^2 function of the coefficient vector $\boldsymbol{c} = \{c_b\}$. χ is defined as below

$$\begin{cases} \chi^2(\boldsymbol{c}) = \sum_s (\boldsymbol{p}_s - f_s \boldsymbol{R}(\boldsymbol{x}_s)\psi)^T \boldsymbol{W}_s (\boldsymbol{p}_s - f_s \boldsymbol{R}(\boldsymbol{x}_s)\psi) \\ \boldsymbol{R}_{ij}(\boldsymbol{x}_s) = h(\boldsymbol{x}_j - \eta.(\boldsymbol{x}_i - \boldsymbol{x}_s)). \end{cases} \tag{6}$$

Here, $\boldsymbol{p}_s$ is the gray distribution of point source s, f_s is its flux within the aperture, $\boldsymbol{W}_s$ is the inverse of the pixel noise covariance matrix for s, and $\boldsymbol{R}(\boldsymbol{x}_s)$ is a resampling factor that depends on the image grid coordinates $\boldsymbol{x}_s$ of the point source centroid. h is a two-dimensional interpolation function, $\boldsymbol{x}_i$ and $\boldsymbol{x}_j$ are the coordinate vectors of image pixel i and model sample j, respectively, and η is the oversampling factor. The complicate optimizing process has been implemented in PSFEx package. In our study, we use PSFEx software directly to obtain the centroids of stars.

In additional, the xPSFs provided by CICLOPS (West et al. 2010; Knowles et al. 2020) are standard numerical models for NAC images. In our experiments, they were used to simulate the gray distribution of real stars in images and iteratively adjust the centroid to make the simulated distribution resemble the real star image. Finally, all star centroids in NAC images were obtained. For simplicity, we refer to this method as the xPSF method.

In summary, for ISS NAC images, we used the three PSF fitting methods (ePSF, PSFEx and xPSF) to obtain all star centroids in images, and then compared the results from the three methods.

3. Experiment

To evaluate the effectiveness of the five centering algorithms, a comparative experiment was performed. The experiment consists of three steps: (1) preparing ISS NAC Images, (2) determining the positions of all reference stars in the images using each of the five centering algorithms, (3) computing the positions of all reference stars in the images based on the star data from Gaia DR3 (Gaia Collaboration et al. 2023), and deriving the residuals between the observed and computed positions.

3.1. Preparing ISS NAC Images

The comparison of various centering algorithms was conducted for astrometry of ISS NAC images, so a collection of star field images captured by the ISS NAC was chosen. The data set consists of all images in the image sequence titled "ISS_026ST_CHARGEXF001_PRIME," which has 70 sequential images taken on 213th day in 2006, numbered from N1533083910 to N1533095430. These images exhibit only minor relative shifts between adjacent frames, as they focus on the same sky region. Each image's size is 1024×1024 pixels and was captured using the combined CL1 and CL2 filters, with an exposure time of 2.6 s. The faintest star magnitude considered in the analysis is 15, leading to about 190 detected stars per image. By analyzing this sequence of star field observations, we can evaluate the centering accuracy and precision of the algorithms being tested for ISS NAC point source measurements.

Generally, each images should be calibrated before measurement. This process includes bias subtraction, dark current correction, flat-fielding, bad pixel masking and so on. Fortunately, the calibrated images for these raw images can be directly downloaded from the NASA Planetary Data System. In addition, when it is necessary to independently determine the sky background, we also use the algorithm proposed by Bertin & Arnouts (1996) in which the mode is taken as background value, where the mode is defined as

$$\begin{cases} \text{Mode} = 2.5 \times \text{Median} - 1.5 \times \text{Mean} & (\text{Mean} - \text{Median})/\text{Std} \leqslant 0.3 \\ \text{Mode} = \text{Median} & (\text{Mean} - \text{Median})/\text{Std} > 0.3. \end{cases} \tag{7}$$

3.2. Measurement of Star Centroids

After preprocessing the images, we employed five different algorithms to determine the centroids of all stars in the images. The Gaussian fitting and modified moments methods have been integrated into the Caviar software (Cooper et al. 2018). We therefore used Caviar to obtain the centroids for all stars in the images from Gaussian fitting and modified moments method.

As mentioned above, PSFEx can construct PSF models and determine star centroids simultaneously through an iterative

Table 1
The Optimized Main Parameters used in the SExtractor and PSFEx Package

Software	Parameter	Value	Description
SExtractor	DETECT_MINAREA	3	Minimum number of pixels above threshold for point sources
	DETECT_THRESH	1.5σ	Selection threshold
	FILTER_NAME	Gauss_2.0_3 × 3.conv	Filter
PSFEx	BASIS_TYPE	default[a]	Basis vector size
	BASIS_NUMBER	default[b]	Size of basis vector set
	PSF_SAMPLING	0.25	Unit pixel sampling grid
	PSF_ACCURACY	0.001	Expected pixel accuracy of the PSF
	PSF_SIZE	21,21	PSF image size

Notes.
[a] The default value is PIXEL_AUTO: NONE (no basis) for properly sampled images and switches automatically to PIXEL (super-resolution) for critically sampled and undesampled data.
[b] The default value is 20: When BASIS_TYPE is PIXEL, it represents square-root of the number of pixels.

Table 2
The Main Parameters used in Photutils

Class	Parameter	Value	Description
DAOStarFind	fwhm	1.3	Full width at half maximum
	threshold	50 × rms	Selection threshold
EPSFBuilder	oversampling	4	Oversampling factor
	maxiters	10	Maximum number of iterations
	fit_boxsize	(5,5)	Fitting sample box size
	recentering_boxsize	(5,5)	Recentering box size for centroid relocation
	smoothing_kernel	quadratic	Model smoothing function

fitting process. Typically, PSFEx is used in conjunction with SExtractor (Bertin & Arnouts 1996). We used SExtractor to extract source coordinates and other relevant information from all images, outputting this data as a catalog file. Subsequently, PSFEx processed this catalog, filtering and iterating to construct the PSF model and calculate the centroids of the stars concurrently. The main parameters used in the SExtractor and PSFEx packages are outlined in Table 1. To achieve best results, we optimized these parameters. Ultimately, a set of star centroids derived from PSFEx was obtained.

Photutils (Bradley et al. 2024) is a Python package that implements the ePSF algorithm. We began by using the DAOStarFinder class, which employs the DAOPHOT algorithm (Stetson 1987), to identify point sources suitable for building the ePSF model in all images. Following edge filtering, coordinate extraction, and image segmentation, we utilized the EPSFBuilder class to construct the ePSF model and obtain the star centroids. The main parameters used in Photutils are outlined in Table 2. These parameters were tailored for our images and optimized for the best results. The final results from the ePSF algorithm were subsequently obtained.

In the xPSF method, we directly used the PSF provided by CICLOPS for fitting measurements. Since our images were all taken with the CL1 and CL2 filters, we employed the *xpsf_nac_cl1_cl2_core* file from CICLOPS, which provides the PSF model corresponding to our conditions. This model is 51×51 pixels in size with a precision of 0.1 pixels. Given that the FWHM is 1.3 pixels, we performed fitting only within a 5×5 pixel neighborhood around the star's center. We iteratively adjusted the star centroid parameters to ensure that the PSF-generated simulated star image closely matched the actual star image, thereby determining the centroids of all stars. For implementation, we used the *IterativelySubtractedPSFPhotometry* class provided by Photutils to simplify programming.

It should be noted that after obtaining the centroids of the stars using the five different centering methods, we applied Owen's geometric distortion model (Owen 2003) to correct these centroids. Consequently, we obtained the geometric distortion-free centroid for each star for each centering algorithm.

3.3. Reduction of Star Centroids

First, based on the nominated camera's pointing (A_0, D_0) at each image's observation time, we match the stars in the image with the stars in the Gaia DR3 (Gaia Collaboration et al. 2023) to obtain their R.A. α and decl. δ in the International Celestial

Table 3
Mean and Standard Deviation of $(O-C)$s for different Plate Constant Models and Centering Algorithms (Unit in pixels)

Plate Constants Model	Direction	ePSF		PSFEx		xPSF		Gaussian		Modified Moments	
		Mean	Std	Mean	Std	Mean	Std	Mean	Std	Mean	Std
6-parameter	Sample	0.001	0.063	0.002	0.081	0.001	0.077	0.001	0.134	0.001	0.068
	Line	−0.005	0.064	−0.007	0.074	−0.006	0.068	−0.001	0.149	−0.005	0.073
12-parameter	Sample	0.001	0.061	0.002	0.081	0.001	0.076	0.001	0.133	0.001	0.066
	Line	−0.004	0.057	−0.005	0.069	−0.004	0.062	−0.000	0.145	−0.003	0.067
20-parameter	Sample	0.001	0.054	0.003	0.076	0.003	0.070	0.001	0.129	0.003	0.060
	Line	−0.004	0.044	−0.005	0.053	−0.005	0.053	−0.001	0.140	−0.003	0.056
30-parameter	Sample	0.001	0.054	0.002	0.076	0.003	0.069	0.001	0.128	0.002	0.059
	Line	−0.004	0.044	−0.005	0.053	−0.005	0.053	−0.000	0.137	−0.003	0.056

Reference Frame. We then correct these coordinates for proper motion, parallax, and light travel time. Subsequently, the Gnomonic Projection is used to convert these corrected celestial coordinates to the standard coordinates (ξ, η) on the tangent plane corresponding to the initial pointing:

$$\begin{cases} \xi = \dfrac{\cos\delta \sin(\alpha - A_0)}{\sin D_0 \sin\delta + \cos D_0 \cos\delta \cos(\alpha - A_0)} \\ \eta = \dfrac{\cos D_0 \sin\delta - \sin D_0 \cos\delta \cos(\alpha - A_0)}{\sin D_0 \sin\delta + \cos D_0 \cos\delta \cos(\alpha - A_0)}. \end{cases} \tag{8}$$

Next, we use a polynomial model to establish the mapping relationship between the tangent plane coordinates (ξ, η) and the image coordinates (x, y). For example, for a 20-parameter model, the equations are as follows:

$$\begin{cases} x = a_0 + a_1\xi + a_2\eta + a_3\xi^2 + a_4\xi\eta + a_5\eta^2 + a_6\xi^3 + a_7\xi^2\eta + a_8\xi\eta^2 + a_9\eta^3 \\ y = b_0 + b_1\xi + b_2\eta + b_3\xi^2 + b_4\xi\eta + b_5\eta^2 + b_6\xi^3 + b_7\xi^2\eta + b_8\xi\eta^2 + b_9\eta^3. \end{cases} \tag{9}$$

For ith star in a single image, we input the image coordinates (x_i, y_i) and the corresponding tangent plane coordinates (ξ_i, η_i) into the above equations. By using the least squares method, we can obtain the 20 parameters in Equation (9). These parameters allow us to use the tangent plane coordinates to calculate the expected image coordinates of each star, representing their true positions in the image.

We then compute the difference between the measured positions and these calculated positions for each star, referred to as the observed-minus-calculated $(O-C)$ residuals. These residuals are used to assess the performance of each of different centering algorithms.

It should be noted that in our experiments, we evaluated different plate constants models, including 6-, 12-, 20-, and 30-parameter models to express the mapping between the tangent plane coordinates and the image coordinates. The results obtained from different models showed some variations, which will be discussed in the next section.

4. Results and Analysis

After obtaining all the $(O-C)$ residuals, we conducted a statistical analysis of the positional measurement residuals for all stars, which were measured using different plate constant models and various centering algorithms. Table 3 presents the statistical results. From the table, it is evident that the ePSF method consistently outperforms other centering techniques in precision across all plate constant models. Among the models with 6, 12, 20, and 30 parameters, the 30-parameter model yields the highest overall measurement precision. However, the 20-parameter model achieves results nearly equivalent to the 30-parameter model. The 20-parameter model can be considered the optimal choice overall, as it offers precision comparable to the 30-parameter model while utilizing fewer parameters, thereby reducing computational complexity and cost.

Next, the detailed measurement results are given for each centering algorithm under the 20-parameter model. Figure 1 shows the standard deviations of residuals in the sample direction, while Figure 2 shows them in the line direction, with the horizontal axis representing magnitude and the vertical axis representing the average standard deviation (in pixels) of target stars within each magnitude interval. Based on both figures, we see that the ePSF method provides the best precision among the five algorithms in sample and line directions, while the Gaussian fitting gives the worst precision.

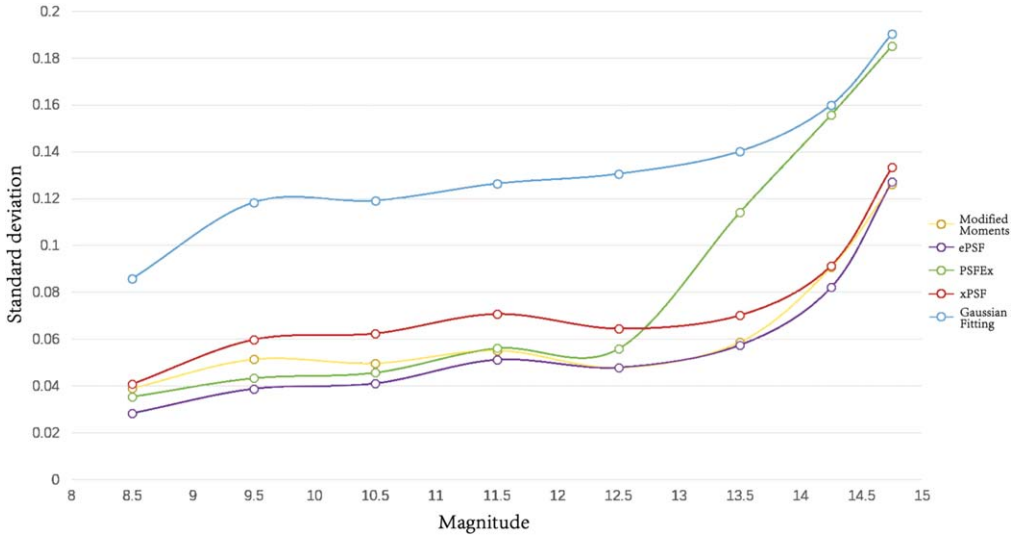

Figure 1. The standard deviations of residuals of each centering method in the sample direction.

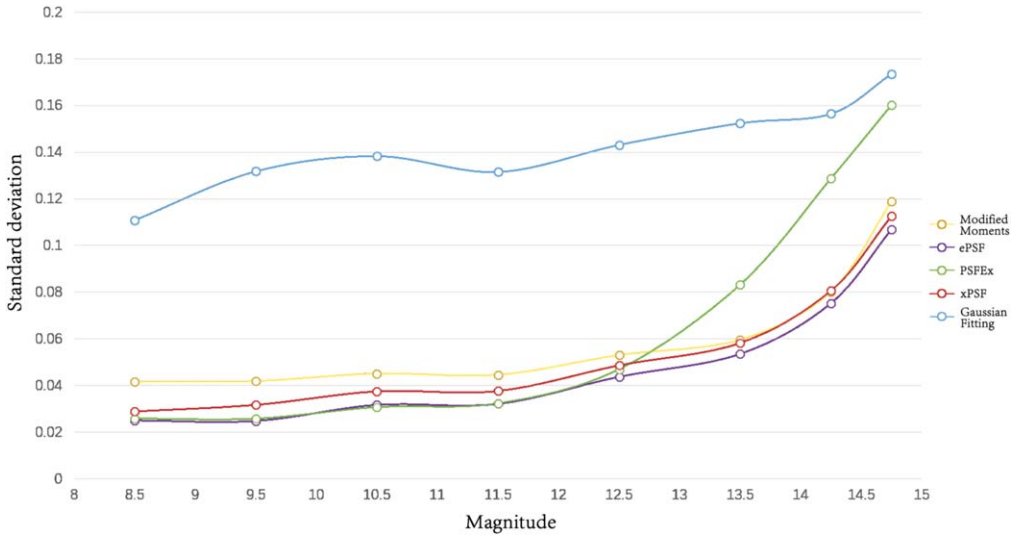

Figure 2. The standard deviations of residuals of each centering method in the line direction.

The results are also presented in Table 4. As shown in the table, the mean values of all residuals for each algorithm across different magnitudes are close to zero, indicating no significant systematic bias. In terms of standard deviation, the ePSF method achieved the smallest values in both the sample and line directions across all magnitude levels. Conversely, the Gaussian fitting method exhibited the worst measurement precision at all magnitude levels. This is understandable, as the NAC ISS images with (CL1, CL2) are undersampled, with an FWHM of only 1.3 pixels. The Gaussian shape cannot accurately represent the true intensity distribution of stars. Overall, the ePSF method achieves a precision of 0.054 and 0.044 pixels in the sample and line directions, respectively. In contrast, the least accurate Gaussian fitting method exhibits significantly poorer performance, with precisions of 0.129 and 0.140 pixels in the respective directions. The three PSF fitting methods demonstrated relatively similar precisions, with the ePSF method performing the best. However, the results obtained from the CICLOPS-provided xPSF model, considered the authoritative PSF model, are worse than expected. The ePSF method surpasses xPSF, showing overall enhancements of about 23% and 17% in the sample and line directions, respectively. Regardless of the method used, measurement precision overall decreases as the magnitude increases.

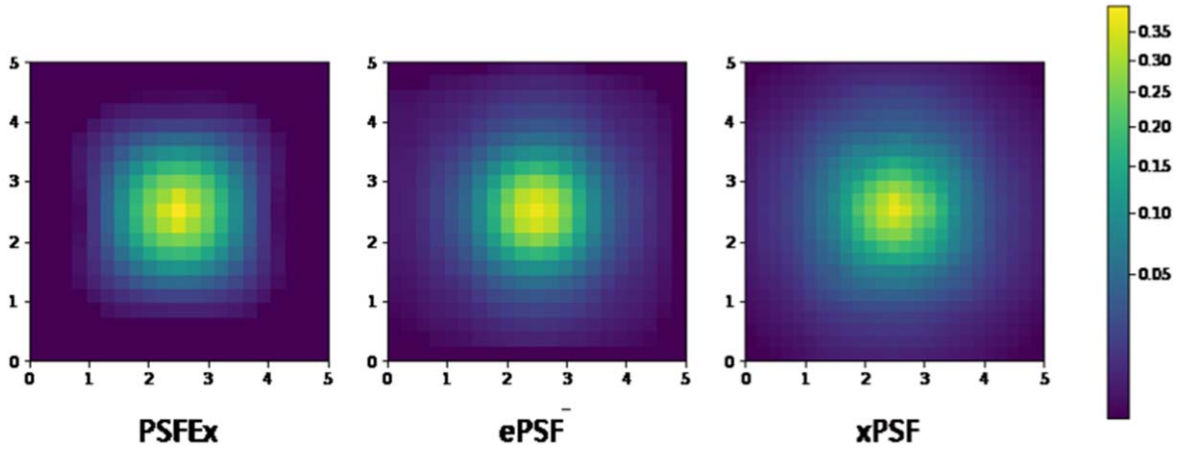

Figure 3. PSF models derived from PSFex, ePSF and xPSF methods.

Table 4
The Mean Values and Standard Deviations of Residuals of Each Centering Method in Sample and Line Directions (Unit in pixels)

Magnitude	Number of Stars	Direction	ePSF		PSFEx		xPSF		Gaussian		Modified Moments	
			Mean	Std	Mean	Std	Mean	Std	Mean	Std	Mean	Std
8–9	210	Sample	0.004	0.029	0.004	0.037	0.005	0.043	−0.001	0.090	0.005	0.041
		Line	−0.018	0.026	−0.020	0.027	−0.020	0.030	−0.003	0.117	−0.019	0.044
9–10	943	Sample	0.006	0.039	0.008	0.043	0.007	0.060	0.009	0.119	0.007	0.052
		Line	−0.020	0.025	−0.023	0.026	−0.022	0.032	−0.011	0.133	−0.018	0.042
10–11	1504	Sample	0.006	0.041	0.008	0.045	0.006	0.062	0.005	0.119	0.008	0.050
		Line	−0.008	0.032	−0.010	0.031	−0.010	0.037	−0.004	0.138	−0.005	0.045
11–12	1511	Sample	0.003	0.051	0.003	0.056	0.002	0.070	0.004	0.126	0.004	0.055
		Line	0.004	0.032	0.001	0.032	0.002	0.037	−0.001	0.132	0.006	0.044
12–13	1803	Sample	−0.003	0.048	−0.002	0.056	−0.003	0.064	−0.001	0.131	−0.004	0.048
		Line	0.009	0.044	0.006	0.047	0.009	0.048	0.010	0.143	0.010	0.053
13–14	2424	Sample	−0.006	0.057	−0.004	0.114	−0.006	0.070	−0.004	0.140	−0.006	0.059
		Line	0.006	0.053	0.009	0.058	0.007	0.083	0.007	0.153	0.005	0.060
14–15	4158	Sample	0.000	0.114	−0.003	0.181	0.000	0.121	−0.002	0.184	−0.001	0.115
		Line	−0.001	0.097	0.002	0.151	0.001	0.103	−0.004	0.170	−0.002	0.107
Overall	12553	Sample	0.001	0.054	0.003	0.076	0.003	0.070	0.001	0.129	0.003	0.060
		Line	−0.004	0.044	−0.005	0.053	−0.005	0.053	−0.001	0.140	−0.003	0.056

Additionally, the measurement precision becomes significantly worse when the star is fainter than magnitude 12.5.

Zhang et al. (2021) considered the modified moments method a good approach, but they did not compare it with PSF fitting methods. In this study, however, it is shown to perform worse than the ePSF method. For faint stars with a magnitude greater than 12.5, the modified method provides similar precision as the ePSF, but for bright stars, it is 0.01 pixels worse. Overall, the ePSF method achieves better precision compared to the modified moments method across all magnitudes. The superior performance of the ePSF method over the modified method is expected, as Anderson & King (2000) noted its benefit for astrometry of undersampled images such as the Cassini ISS NAC images.

The inferior results of the xPSF method compared to the ePSF method were unexpected, especially considering the authoritative status of the xPSF model from CICLOPS. This discrepancy likely arises because the xPSF is generated for accurate photometry rather than astrometry, unlike the ePSF which is optimized for astrometry. This highlights the need to produce PSF models specifically tailored for astrometric purposes. For visual comparison, we have included the PSF models derived from ePSF and PSFEx alongside the xPSF in Figure 3. These models are scaled uniformly to a 5×5 pixel

range, which is sufficient for centering point sources in ISS NAC images. The figure shows that all three models are very similar, but the xPSF model appears sharper than the others. Experimental results indicate that the ePSF model performs best. To facilitate high-precision astrometry for NAC images with CL1 and CL2 filters, we have published the ePSF model on GitHub (https://github.com/Astrometry-JNU/ePSF_model).

5. Conclusion

This study conducted a comparative analysis of five centering algorithms (Gaussian fitting, modified moments, ePSF, PSFEx, and xPSF) using NAC images with the (CL1, CL2) filter combination. The results show that the ePSF method achieved the best measurement precision across all magnitude ranges. For stars of magnitude 8–9, a precision better than 0.03 pixels was attained. The measurement precision declined as the stars became fainter, reaching around 0.1 pixels for the faintest 14–15 mag stars. Overall, the measurement precision reached 0.054 pixels in the sample direction and 0.044 pixels in the line direction. These values represent an improvement of approximately 10% and 21%, respectively, over the previously considered best-performing modified moments method in the two directions.

Because the NAC images are undersampled, the PSF fitting method is anticipated to provide superior measurement precision. The xPSF, recognized as the standard PSF model for the NAC by CICLOPS, is expected to offer excellent measurement accuracy in theory. Nonetheless, experimental results have demonstrated that the ePSF method surpasses xPSF, showing overall enhancements of about 23% and 17% in the sample and line directions, respectively. This discrepancy mainly stems from the fact that xPSF was designed with a photometric focus, lacking optimization for positional measurements. This finding suggests that the NAC's PSFs should be reconstructed to achieve high-precision positional measurements. Thoroughly investigating the NAC images and constructing additional PSF models of NAC with other filters combinations for high-precision astrometry is necessary in the future. To assist researchers, we have made the PSF model for NAC with the (CL1, CL2) filter combination available for download on GitHub.

Acknowledgments

This work has been partly supported by the National Natural Science Foundation of China (No. 12373073, U2031104, No. 12173015), Guangdong Basic and Applied Basic Research Foundation (No. 2023A1515011340). This work has made use of data from the European Space Agency (ESA) mission Gaia (https://www.cosmos.esa.int/gaia), processed by the Gaia Data Processing and Analysis Consortium (DPAC, https://www.cosmos.esa.int/web/gaia/dpac/consortium). Funding for the DPAC has been provided by national institutions, in particular the institutions participating in the Gaia Multilateral Agreement. We would also like to express our gratitude to Nick Cooper for his invaluable assistance in improving the English of this manuscript. His suggestions greatly enhanced the clarity and quality of this paper.

References

Anderson, J., & King, I. R. 2000, PASP, 112, 1360
Auer, L. H., & van Altena, W. F. 1978, AJ, 83, 531
Bertin, E. 2011, ASP Conf. Ser. 442, Astronomical Data Analysis Software and Systems XX, ed. I. N. Evans et al. (San Francisco, CA: ASP), 435
Bertin, E., & Arnouts, S. 1996, A&AS, 117, 393
Bradley, L., Sipőcz, B., Robitaille, T., et al. 2024, astropy/photutils: v1.13.0
Cooper, N. J., Lainey, V., Meunier, L. E., et al. 2018, A&A, 610, A2
Cooper, N. J., Murray, C. D., Lainey, V., et al. 2014, A&A, 572, A43
Cooper, N. J., Murray, C. D., Porco, C. C., & Spitale, J. N. 2006, Icar, 181, 223
Gaia Collaboration, Vallenari, A., Brown, A. G. A., et al. 2023, A&A, 674, A1
Jia, P., Wu, X., Yi, H., Cai, B., & Cai, D. 2020, AJ, 159, 183
Knowles, B., West, R., Helfenstein, P., et al. 2020, P&SS, 185, 104898
Lainey, V., Rambaux, N., Tobie, G., et al. 2024, Natur, 626, 280
Lu, T., Luo, W., Zhang, J., et al. 2018, AJ, 156, 14
Owen, W. M., Jr. 2003, JPL IOM 312.E-2003-001 (Flintridge, CA: Jet Propulsion Laboratory)
Porco, C. C., West, R. A., Squyres, S., et al. 2004, SSRv, 115, 363
Stetson, P. B. 1987, PASP, 99, 191
Stone, R. C. 1989, AJ, 97, 1227
Tajeddine, R., Cooper, N. J., Lainey, V., Charnoz, S., & Murray, C. D. 2013, A&A, 551, A129
Tajeddine, R., Lainey, V., Cooper, N. J., & Murray, C. D. 2015, A&A, 575, A73
West, R., Knowles, B., Birath, E., et al. 2010, P&SS, 58, 1475
Zhang, Q. F., Lainey, V., Cooper, N. J., et al. 2018, MNRAS, 481, 98
Zhang, Q. F., Qin, W. H., Ma, Y. L., et al. 2022, P&SS, 221, 105553
Zhang, Q. F., Zhou, X. M., Tan, Y., et al. 2021, MNRAS, 505, 5253
Zhang, Z. Y., & Peng, Q. Y. 2010, AR&T, 7, 132